LAWRENCE
LIVERMORE
NATIONAL
LABORATORY

LLNL-JRNL-822758

Protein-based platform for one-step purification , chelation, and study of medical radiometals: yttrium and actinium

G. Deblonde, J. Mattocks, Z. Dong, J. Cotruvo, M. Zavarin

May 19, 2021

Science Advances

Disclaimer

Title: Capturing an elusive but critical element: Natural protein enables actinium chemistry

Short title: Enabling actinium chemistry using lanmodulin

Authors

Gauthier J.-P. Deblonde[1,2*], Joseph A. Mattocks[3], Ziye Dong[1], Paul T. Wooddy[1], Joseph A. Cotruvo, Jr.[3*], Mavrik Zavarin[1,2]

* Corresponding authors: Deblonde1@LLNL.gov (GJPD) and juc96@psu.edu (JAC)

Affiliations

[1]*Physical and Life Sciences Directorate, Lawrence Livermore National Laboratory, Livermore, California 94550, United States.*

[2]*Glenn T. Seaborg Institute, Lawrence Livermore National Laboratory, Livermore, California 94550, United States.*

[3]*Department of Chemistry, The Pennsylvania State University, University Park, Pennsylvania 16802, United States.*

Abstract

Actinium-based therapies could revolutionize cancer medicine but remain tantalizing due to the difficulties in studying and limited knowledge of Ac chemistry. Current efforts focus on small synthetic chelators, limiting radioisotope complexation and purification efficiencies. Here we demonstrate a straightforward strategy to purify medically-relevant radiometals, actinium(III) and yttrium(III), and probe their chemistry, using the recently discovered protein, lanmodulin. The stoichiometry, solution behavior, and formation constant of the $^{228}Ac^{3+}$-lanmodulin complex (Ac_3LanM, K_d = 865 femtomolar) and its $^{90}Y^{3+}/^{nat}Y^{3+}/^{nat}La^{3+}$ analogues were experimentally determined, representing both the first actinium-protein and most stable actinide(III)-protein species to be characterized. Lanmodulin's unparalleled properties enable the facile purification-recovery of radiometals, even in the presence of $>10^{+10}$ equivalents of competing ions and at ultra-trace levels: down to 2 femtograms $^{90}Y^{3+}$ and 40 attograms $^{228}Ac^{3+}$. The lanmodulin-based approach charts a new course to study elusive isotopes and develop versatile chelating platforms for medical radiometals, both for high-value separations and potentially *in vivo* applications.

Teaser: Demystifying the elusive chemistry of actinium leads to novel opportunities in radioisotope production and nuclear medicine

INTRODUCTION

The use of radionuclides in medicine has been continuously growing over the past decades, especially in the case of short-lived radiometals, as they are among the most efficient means for

medical imaging (e.g., PET and SPECT scans) and treatment of a wide array of diseases (e.g., bone metastasis, prostate cancers, and non-Hodgkin's lymphoma) (*1–4*). In particular, actinium (Ac^{3+}) is largely seen as the most promising candidate for next-generation cancer treatments, *i.e.* targeted alpha therapy (*3*, *5*, *6*). The nuclear properties of ^{225}Ac make it an ideal projectile against tumor cells (Figure S1): ^{225}Ac is a rare case of an alpha emitter with only short-lived daughters, decaying without leaving radioactive materials in the patient's body; its 9.95-day half-life is suitable for medical applications; and its decay chain delivers, on average, 4 high-energy alpha plus 2 beta particles – leading to treatment efficacy hundreds of times higher (*7–9*) than current medical radiometals. Therefore, if successful, the combined large-scale production, purification, and assembly of ^{225}Ac pharmaceuticals has the potential to revolutionize cancer medicine.

However, no ^{225}Ac-based drug has reached the market because of significant scientific challenges, from isotope production to the design of specific chelators for radiolabeled drugs. In fact, Ac^{3+} chemistry remains largely unknown compared to cations currently used in medicine (Ga^{3+}, Zr^{4+}, $Tc^{5+/7+}$, Y^{3+}, Gd^{3+}, Lu^{3+}, Sc^{3+}, In^{3+}…) or other heavy radioelements for oncology ($^{223}Ra^{2+}$, $^{227}Th^{4+}$…) (*10*, *11*), or even synthetic actinides discovered decades after actinium (Np, Pu, Am…), which impairs the development of any application involving actinium. For example, only very recently was the coordination number of Ac^{3+} in HCl solution determined (*12*), and only a handful of Ac^{3+} complexes have been thermodynamically characterized, all with simple ligands (e.g. $AcCl_3$, AcF_3 $[Ac(C_2O_4)_2]^-$, $[AcEDTA]^-$) (*13*). Additionally, since only one Ac^{3+} complex with a small organic chelator has ever been isolated (*i.e.,* $Ac_2(C_2O_4)_3{\cdot}nH_2O_{(s)}$ (*14*, *15*)) and partially characterized via powder X-ray diffraction, the properties of Ac complexes are typically extrapolated from those of the easier to study analogs with lanthanides and heavy actinides (Am^{3+}, Cm^{3+}). Another barrier is the low availability of all Ac materials, even at the research scale. All Ac isotopes are radioactive (Figure 1a). The longest-lived one, ^{227}Ac (21.8 years), would be suitable for chemical studies but it is cost prohibitive (>1,000 USD/microgram), difficult to produce and

purify, and requires specialized handling (*i.e.*, a glovebox), even relative to many other radioisotopes (*16*, *17*). ^{225}Ac is the main focus of medical research and multiple production routes are being investigated worldwide as the current isotope availability is much lower than the projected demand. Current production methods require large instruments like particle accelerators, cyclotrons, or necessitate decades-old legacy nuclear materials, limiting ^{225}Ac availability. In addition, access is largely limited to clinical development rather than the fundamental studies of Ac^{3+} chemistry that would be helpful to better design those clinical applications (*16*, *18–21*). The ^{235}U/^{231}Pa and ^{233}U/^{229}Th decay chains include ^{227}Ac and ^{225}Ac, respectively, but these radionuclides have very long secular equilibrium periods (Figure S1, Table S1) and present nuclear proliferation issues, so they are tightly controlled and unlikely to make actinium more accessible. Consequently, there is no widely available generator from which Ac isotopes could be periodically extracted, forcing research laboratories willing to embark on actinium studies to purchase limited, expensive, and short-lived ^{225}Ac sources.

By contrast, $^{228}Ac^{3+}$ (6.1 hours) occurs in the decay chain of $^{232}Th^{4+}$, an inexpensive radioisotope that is abundant and already available at numerous industrial sites and research institutions. $^{228}Ac^{3+}$ has been largely overlooked due to the lack of practical extraction methods since the mass of actinium isotopes in aged radioactive sources is extremely low (Table S1). After 10 years, 1 gram of ^{232}Th only contains ~3.5×10^{-14} g of ^{228}Ac – enough for radiochemical studies but beyond the capabilities of current Ac chelators. ^{228}Ac could become the most accessible Ac isotope and help to develop Ac chemistry as a whole, but only if an efficient and practical purification method can be implemented.

Here, we show that such a method can be realized using the protein lanmodulin (LanM), the first natural macrochelator selective for rare earth elements to be discovered, in 2018 (*22*). Taking advantage of LanM's size, selectivity, and affinity, we purify $^{228}Ac^{3+}$ and also $^{90}Y^{3+}$, a rare earth radioisotope currently in clinical use in medical PET and SPECT imaging, from their generators

($^{232}Th^{4+}/^{228}Ra^{2+}$ and $^{90}Sr^{2+}$, respectively) with unprecedented ease of implementation (Figure 1B-C). Furthermore, our method allows us to study the chemistry of Ac^{3+} with LanM – by far the most complex ligand for Ac^{3+} characterized to date – and other relevant bio-ligands for the first time. These studies reveal a higher affinity even than for the protein's natural substrates (lanthanides) and the highest stability constant reported for any Ac^{3+} complex, small molecules included (*13*). Because many radiometals are trivalent rare earths or actinides that LanM selectively binds and that would otherwise require cumbersome purification processes, our work suggests a general strategy for rapid radioisotope purification, detection, study, and perhaps even theranostic applications.

RESULTS

Macromolecular purification of radioisotopes. The use of biomacromolecules, such as proteins, has largely been absent from purification strategies targeting radiometals like yttrium and actinium, as most known metal-binding proteins are not selective for f-elements (*23–25*). Even previous studies investigating interactions of proteins with uranium or heavy actinides (plutonium, americium, curium…) (*26–28*) have largely focused on bacterial and human iron or calcium transport machineries, which not only form relatively weak complexes with trivalent f-elements but also only operate under a very narrow set of conditions (typically pH >6 and requiring a synergistic ligand like a carbonate or a siderophore molecule). By contrast, LanM displays unprecedented selectivity for trivalent lanthanides against most other cations (*22*, *29*, *30*). Instead of using minor differences in extraction reaction constants (as with current extractants, resulting in arduous metal ion separations (*16*, *17*)), a selective macromolecular extractant such as LanM (~12 kDa, hydrodynamic radius ~4 nm (*30*)) would enable a new and more robust mechanism for recovery and purification of radiometals based on size differences. We hypothesized that protein-bound versus unbound metal ions could easily be separated using inexpensive methods like spin filtration or size exclusion chromatography (Figure 1b-c).

Short-lived radioisotopes require special handling but their actual concentration is very low (Table S1), necessitating extremely efficient and selective metal-binding molecules. To evaluate the protein-based radioisotopes purification strategy, we first attempted to recover $^{90}Y^{3+}$ from $^{90}Sr^{2+}$ sources using LanM. $^{90}Y^{3+}$ is used for radioimmunotherapy and medical imaging (SPECT/CT, gamma, PET…) (*31*, *32*). $^{90}Sr^{2+}$ has a long half-life (28.9 years) and β-decays to $^{90}Y^{3+}$ (2.66 days). At secular equilibrium, the ratio $^{90}Sr^{2+}/^{90}Y^{3+}$ is ~4,000 mol/mol. The $^{90}Sr^{2+}/^{90}Y^{3+}$ pair can be used as a generator for the short-lived $^{90}Y^{3+}$ but, despite a sufficient stockpile of $^{90}Sr^{2+}$, its global deployment has been hindered by difficulties in separating these isotopes efficiently, rapidly, and inexpensively (*33*).

Figure 2a-d show the LanM-driven separation obtained after a single elution of an aqueous solution at pH 7 containing a mixture of $^{90}Sr^{2+}/^{90}Y^{3+}$, initially at secular equilibrium. Efficient and quantitative separation of the two isotopes was observed after a single step and without requiring any eluant variation, loading/washing/elution cycles, or highly acidic extraction conditions. Such separation takes <5 min and could be even faster if automated. The presence of $^{90}Y^{3+}$ in the high-molecular-weight fraction and $^{90}Sr^{2+}$ in the low-molecular-weight fraction was confirmed by monitoring the activity of the samples by liquid-scintillation counting (Figure 2b-d). The decay profiles of the protein fraction (Figure 2c) and small-molecule fraction (Figure S2) match exactly those of pure $^{90}Y^{3+}$ and $^{90}Sr^{2+}$, respectively. The energy spectra of the protein and low-molecular-weight fractions also match the fingerprints of the high-energy β emitter ^{90}Y and low-energy β emitter ^{90}Sr, respectively (Figure 2d). After this one-step separation, the radiopurity of ^{90}Y increases from 50% to 99.9% (Figure S3). The robustness of the LanM-based separation method and stability of the protein against radiolysis was also evaluated. No decrease in separation performance was observed even when exposing LanM to $^{90}Sr/^{90}Y$ at 5 μCi/mL for a period of 150 hours (Figure S4). Similar attempts to separate $^{90}Y^{3+}$ and $^{90}Sr^{2+}$ using human apo-transferrin – a protein considered as the main f-element transporter in mammals (*27*, *34*, *35*) – failed due to the lower affinity and lack

of selectivity of transferrin relative to LanM. Even under optimal conditions and at transferrin concentrations well above the level found in the bloodstream, less than 10% binding to $^{90}Y^{3+}$ was observed (Figure S5), highlighting that LanM is much more effective and selective than previously known lanthanide-binding proteins.

The efficiency and selectivity of LanM for $^{90}Y^{3+}$ chelation suggests that it could be leveraged to complex actinium, even for its very short-lived isotope, $^{228}Ac^{3+}$. Commercially available $^{232}Th^{4+}$ salts exhibit measurable activity of $^{228}Ac^{3+}$ after a few months (Figure S6), albeit at extremely low concentration (Table S1). Being able to selectively recover $^{228}Ac^{3+}$ could make Ac chemistry readily available and independent from the cost-prohibitive and scarce $^{227/225}Ac$ sources. The $^{232}Th^{4+}$ decay chain comprises $^{228}Ra^{2+}$ (5.7 years) which decays to $^{228}Ac^{3+}$, then $^{228}Th^{4+}$ (1.9 years) and $^{224}Ra^{2+}$ (3.6 days) (Figure S1). Starting from a $^{232}Th^{4+}$ nitrate solution, neutralization to pH 6-8 precipitates $^{232}Th^{4+}$ and $^{228}Th^{4+}$ as hydroxide, and co-precipitates the initial $^{228}Ac^{3+}$, leaving the two radium isotopes in solution. Without regeneration by $^{228}Th^{4+}$, $^{224}Ra^{2+}$ and its daughters naturally decay within ~20 days (Figure S7). $^{228}Ra^{2+}$ regenerates $^{228}Ac^{3+}$ within ~30 hours, due to secular equilibrium, so it represents a potential $^{228}Ra^{2+}/^{228}Ac^{3+}$ generator. Our process is shown in detail in Figure S8.

Little information has been published on the recovery of $^{228}Ac^{3+}$ from macroscopic amounts of $^{232}Th^{4+}$, besides a recent liquid-liquid extraction method performed in concentrated HNO_3 media (*36*), and an ion-exchange protocol including >30 steps (*37*) (Figure S9), which we deemed impractical for such a short-lived radioisotope. The liquid-liquid extraction method developed by Kazakov and co-workers (*36*) consists of a multi-stage process where a ^{232}Th(IV) salt is first dissolved in 4 M HNO_3, and then three consecutive liquid-liquid extraction batches are performed using the extractant di(2-ethylhexyl)phosphoric acid and toluene as diluent (each batch necessitating 3 steps: mixing, centrifugation, and phase separation using a funnel), followed by two column chromatography separations, and an evaporation to dryness and redissolution step (Figure

S9A). The ion-exchange protocol developed by Aldrich et al. (*37*) is even more complicated as it requires 4 ion-exchange resin separations as well as 9 evaporation-redissolution operations (Figure S9B). Both methods also produce an acidic solution of ^{228}Ac whose pH conditions must be further adjusted before use for biological applications. The variety and complexity of the operations involved in these conventional hydrometallurgical methods (liquid-liquid extraction in acidic media, evaporation to dryness…) preclude their implementation for a fast, convenient, and periodic harvesting a short-lived radioisotopes such as ^{228}Ac. Additionally, we experimentally observed that the activity of $^{228}Ra^{2+}/^{228}Ac^{3+}$ solutions increases after ~28 days due to reformation of $^{228}Th^{4+}$ from $^{228}Ra^{2+}$ – a phenomenon predicted by the Bateman equation but overlooked in the literature – rendering previously proposed $^{228}Ra^{2+}/^{228}Ac^{3+}$ generators rapidly inoperable (Figure S7). By contrast, our LanM-based size-exclusion method offers direct, rapid, and practical extraction and purification of $^{228}Ac^{3+}$ (Figure 2e-h). In none of the conditions tested did we observe interactions between Ra^{2+} and LanM, yielding high-purity ^{228}Ac(III)-lanmodulin fractions, as confirmed by radioactive decay monitoring and spectral identification (liquid scintillation and gamma spectroscopy – Figure 2h, Figure S3, Figure S10), even when starting from ~8,200 equivalents of $^{228}Ra^{2+}$ or $^{224}Ra^{2+}/^{228}Ra^{2+}/^{228}Ac^{3+}$ mixtures (Figure S11).

We were able to prepare $^{228}Ac^{3+}$ solutions with ≥99.5% radiopurity (99.9% for $^{90}Y^{3+}$) on a daily basis, and at low cost, paving the way for investigating Ac^{3+} chemistry. Similar to $^{90}Y^{3+}/^{90}Sr^{2+}$, attempts to recover actinium using transferrin were unsuccessful (Figure S5). These results establish that LanM uniquely enables practical purification of valuable radioisotopes from generators, making $^{90}Y^{3+}$ and $^{228}Ac^{3+}$ more accessible for medical and chemical studies, and potentially extendable to other isotopes.

Lanmodulin enables facile detection of radiometals even at ultra-trace levels. To demonstrate the efficacy of the LanM-based extraction system and evaluate its limits, tests were performed with metal concentrations in the sub-nanomolar range, mimicking nuclear medicine conditions (*7*).

Single-step separations of $^{228}Ra^{2+}/^{228}Ac^{3+}$ and $^{90}Sr^{2+}/^{90}Y^{3+}$ mixtures were performed using just 1 µM LanM at pH 7 and without sample pre-concentration. Even under these unfavorable conditions for metal binding, LanM enables the efficient and selective scavenging of $^{228}Ac^{3+}$ and $^{90}Y^{3+}$. The $^{90}Y^{3+}$ recovery yield in the protein fraction was maintained at >75% for concentrations as low as ~45 fM, or just ~2 femtograms of yttrium (Figure 3a). Below this level, uptake of $^{90}Y^{3+}$ by LanM was still observed, albeit with a lower yield (50-60%). Even more remarkably, LanM has higher affinity for actinium, and it allows its selective recovery to a concentration as low as 0.3 fM – just 40 attograms under the studied conditions (Figure 3b). Of note, this extremely low mass was only twice the instrumental quantification limit for ^{228}Ac so that more dilute samples were not investigated, but it is likely that the proposed LanM-based system works at even lower Ac^{3+} levels (Figure S12).

Furthermore, the metal uptake reactions with LanM are fast. After only a 5-minute incubation at room temperature and neutral pH, the Ac^{3+}-LanM binding reaction is almost complete (Figure 3c-e). The results reinforce that the LanM-based approach could enable faster, more efficient, and low-cost purification of radioisotopes for medicine and research. It could also be adapted for the field-deployable analysis of radioisotopes, especially f-elements resulting from nuclear activities.

Solution thermodynamics of actinium-lanmodulin. The combined preparation of $^{228}Ac^{3+}$ solutions, efficient binding to LanM, and separation of the LanM complexes from small molecules afford a unique opportunity to probe the chemistry of actinium. While solution chemistry and crystallographic studies have been performed on f-element/protein species since the 1960's (*38*, *39*), including with heavy actinides (*40*, *41*), no actinium-protein complex has ever been characterized, even from a solution thermodynamic standpoint. This situation is due to the low availability of Ac isotopes, lack of Ac^{3+}-specific spectroscopic features, and incompatibility of proteins with classic techniques used for radiotracers, like liquid-liquid extraction (*42*, *43*). Even

for small Ac^{3+} complexes, no stability constant has been experimentally determined since the 1970's, with the strongest species reported being $[AcEDTA]^-$ ($\log \beta_{11} = 14.2$) (*13*, *44*).

Here, we developed a combined radiochemical and size exclusion chromatography method relying on the natural dissociation of metal-chelator complexes at low concentration (Methods). To establish the method, the formation constant of $^{90}Y_3$LanM ($\log \beta_{31}$) was determined to be 33.9(±0.5) at pH 7, corresponding to an average dissociation constant (K_d) of 4.3(±1.5) pM per binding site (Figure 4a-b, Table S2). This value is in excellent agreement with results obtained using non-radioactive yttrium ($K_{d,app}(^{nat}Y_3$LanM) = 4.1±0.3 pM. Figure S13) in ligand-protein titrations followed by circular dichroism (CD), confirming the applicability of the radiometry/dilution-based method. CD cannot be applied to actinium as each experiment would require milligram quantities of the element (>1,000× the current world's supply) and the stability constants between Ac^{3+} and the competing ligand, which are currently unknown (*13*). By contrast, the radiometry/dilution-based experiments only require femtograms of the radioisotope, and do not require a competing ligand. This approach revealed that LanM has very strong affinity for Ac^{3+}, with a $\log \beta_{31}$ of 36.2±0.5 for $^{228}Ac_3$LanM at pH 7, equivalent to an average K_d of 865 fM per site (Figure 4c-f). We previously showed (*22*, *30*, *45*) that lanthanide ions form polymetallic complexes with LanM, Ln_3LanM, at macroscopic concentrations (micromolar to millimolar range). However, LanM has four potential metal binding sites (*22*) and it was unclear whether the fourth site could play a role in the binding of actinium. Combining the results obtained by the dilution-induced dissociation technique and speciation calculations confirms that the actinium-LanM complex is Ac_3LanM (Figure S14). Ac_3LanM is not only the first polynuclear actinium species to be studied, but it also represents the most stable actinide(III)-protein complex.

CD experiments using La^{3+}, a non-radioactive Ac^{3+} analogue, yielded a $K_{d,app}$ of 1.8(±0.1) pM for $^{nat}La_3$LanM (Figure S13). The sub-picomolar stability of Ac_3LanM extends a trend previously noted for the early lanthanides(*22*, *30*) where LanM displays higher affinity for cations with lower Lewis

acidity (Figure 4f). This reversed preference is remarkable when compared to small chelators (*46*) used in medicine since they typically exhibit decreasing affinity (*47*) as the metal gets larger (Figure S15), leading to weak La^{3+} or Ac^{3+} complexes. LanM's combination of high Ac^{3+} affinity, fast kinetics, and selectivity are unparalleled when compared to ligands currently used in clinical studies. For instance, DOTA, which is largely seen as the gold standard for medical radiometals, exhibits slow kinetics and requires elevated temperatures (>70°C) (*48*, *49*) to trigger metal chelation, hindering procedures involving biomolecules. From a thermodynamic perspective, DOTA and other small chelators are also orders of magnitude less selective than LanM for Ac^{3+} against cations naturally present in the bloodstream (Figure S16). Hence, contrary to what has been observed for small f-element complexes used in medicine (*50–52*), Ac_3LanM is inherently less prone to *in vivo* dissociation via transmetallation reactions. Moreover, LanM's multiple binding sites enable multi-isotope radiolabeling (verified here with $^{90}Y^{3+}/^{228}Ac^{3+}$, Figure S17-18), which could allow theranostic strategies using a single chelator. The thermodynamic stability of Ac_3LanM also makes it resistant against endogenous metal-binding proteins like transferrin, whose two binding sites can accommodate trivalent f-elements (*27*, *34*, *53*). While the stability of the Ac_2-transferrin complex has never been measured, a literature review allowed its estimation based on an empirical correlation: log β(Ac_2-transferrin) = 10.9±2, or K_d = 3.5 μM (Figure S19). Despite the large uncertainty inherent to the latter estimation, LanM's affinity for actinium is clearly several orders of magnitude higher than that of transferrin, and transferrin is unable to bind to Ac^{3+} at low concentrations (Figure S12), which is in line with experimental observations. The results suggest that LanM could be the basis for new actinium pharmaceuticals, if sufficiently kinetically inert.

Probing actinium chemistry using lanmodulin. The solution behavior of $^{228}Ac_3$LanM and $^{90}Y_3$LanM was also evaluated. Size-exclusion chromatography assays showed that both complexes are resistant to acidic conditions, with LanM releasing its radioisotopes only below pH ~2.8 (Figure 5a-b). Fitting of the binding curves as a function of pH using the Hill equation yields a high Hill

coefficient (18.2 for Ac and 17.6 for Y). The sharp release of the metal upon acidification further supports the binding of Ac^{3+} (and Y^{3+}) to the three binding sites of LanM. Following selective binding to LanM, both radiometals and protein can be recovered for further use by either lowering pH or adding a chelator in excess; we prepared HCl, HNO_3 as well as EDTA and DTPA solutions of $^{228}Ac^{3+}$, with quantitative yield via one-step spin filtration from $^{228}Ac_3$LanM (Figure S20).

Extending our observation that neither $^{228}Ra^{2+}$ or $^{90}Sr^{2+}$ interact significantly with LanM, LanM's chelation of Ac^{3+} and Y^{3+} is also not impacted by the presence of cations that are ubiquitous *in vivo* and which interact with endogenous proteins and small chelators: Ca^{2+}, Mg^{2+}, Mn^{2+}, Zn^{2+}, and Cu^{2+}. The use of short-lived $^{228}Ac^{3+}$ and $^{90}Y^{3+}$ allowed testing LanM's selectivity with mixtures containing up to 3×10^{11} mol equivalents of each competing cation (Figure 5c). Even under these extreme conditions, selective uptake of Ac^{3+} by LanM was still observed. For $^{90}Y_3$LanM, a slight decrease in radiolabeling yield occurs above a billion-fold excess of divalent cations, corroborating the higher stability determined for $^{228}Ac_3$LanM versus $^{90}Y_3$LanM. Chelators currently used in nuclear medicine are unable to sustain such an excess of competing ions (Figure S16).

Interestingly, differences were observed between Ac^{3+} and Y^{3+} relative to their interactions with small anions present in the bloodstream (Figure 5D-H). A high concentration of sulfate, acetate, or glycine does not destabilize $^{228}Ac_3$LanM or $^{90}Y_3$LanM. However, at high concentration, carbonate and selenite ions compete with LanM and decrease its radiolabeling efficiency for ^{90}Y whereas Ac_3LanM is unaffected. In the case of phosphate ions, $^{228}Ac_3$LanM was found more sensitive than $^{90}Y_3$LanM. The observed trends ($PO_4^{3-} > CO_3^{2-} \approx SeO_3^{2-}$ for actinium versus $CO_3^{2-} > SeO_3^{2-} > PO_4^{3-}$ for yttrium) shed light on subtle chemical differences between actinium and rare earth elements that could be leveraged for separation purposes.

While the direct interactions between Ac^{3+} and carbonate, selenite, or phosphate ions have never been probed under biorelevant conditions, our results indicate that Ac^{3+} exhibits stronger interactions with softer oxygen donors. In line with our experimental results, recent density

functional theory calculations (*54*) showed that replacing DOTA's carboxylate groups by phosphonate groups would impart enhanced stability for the Ac^{3+} complex. However, the design of new actinium complexants should also take into account the selectivity against natural cations, a challenge for most small molecules. Considering LanM's advantages relative to these chelators (e.g., fast kinetics, high selectivity and affinity, pH stability) we posit that the introduction of softer residues in LanM could lead to even more suitable Ac^{3+} macrochelators. Finally, challenging 2 μM La^{3+}-LaMP1, a LanM-based fluorescent sensor ($K_{d,app}$= 9.4 pM) (*29*), with 50% human serum at 37ºC reveals ~5% loss of fluorescence response over 24 h, indicating only minimal metal dissociation (Figure 5H, Figure S21**)**. Given that Ac_3LanM is ~10-fold tighter than La_3LaMP1, these results suggest that Ac^{3+}-LanM may be sufficiently stable for *in vivo* applications.

DISCUSSION

This study represents the first characterization of an actinium-protein complex, $^{228}Ac_3$LanM, as well as experimental study of coordination preferences of Ac^{3+} that previously have largely been probed computationally. Our LanM-based separation strategy allows the efficient, practical, and concomitant chelation/purification of actinium (and $^{90}Y^{3+}$), down to the femtomolar level. The simplicity of our approach, starting from abundant and relatively available starting materials and requiring minimal steps, promises to make $^{228}Ac^{3+}$ more available for fundamental research and chelator development. Furthermore, the short half-life of ^{228}Ac relative to other actinium isotopes means that ^{228}Ac is the most stringent test for the affinity and selectivity of the LanM-based system, such that this approach should be extendable to purification of other actinium isotopes, such as the medically valuable $^{225}Ac^{3+}$ from $^{229}Th^{4+}$ or $^{232}Th^{4+}$. In addition, this biomacromolecular strategy is likely translatable for production of other medically relevant radiometals such as $^{44/47}Sc^{3+}$, purification and detection of strategic actinides such as $^{241}Am^{3+}$ and $^{244}Cm^{3+}$, and study of other elusive elements, notably Es^{3+}, Fm^{3+}, and Md^{3+}, of which several picograms can be produced but which have remained inaccessible with current methodologies. Finally, the stability of LanM's complex with actinium is similar (in fact slightly tighter) to those of its native substrates

(lanthanides), and in the same range as siderophores considered to play a role in the mobilization of actinides and radiolanthanides in the environment (*55*). Therefore, our results raise questions about the influence of natural proteins such as LanM on the binding and transport of natural or anthropogenic radionuclides in the environment. Just as LanM has helped to incorporate the lanthanides into the bioinorganic periodic table, it promises to facilitate understanding of the interactions between actinides and biological systems, as well as the development of the chemistry of actinium and other rare isotopes for both fundamental research and applications in medicine.

MATERIALS AND METHODS

Caution! *^{90}Sr and ^{232}Th, and concentrates of their decay products (^{228}Ra, ^{228}Ac, ^{228}Th…), constitute serious health hazards because of their radioactive and chemical properties. Radiochemical experiments were conducted at LLNL in laboratories designed for the safe handling of short-lived and long-lived radioactive materials and associated waste.*

Materials. Starting $^{90}Sr^{2+}$/$^{90}Y^{3+}$ solutions were prepared by dilution of a primary standardized stock (Eckert & Ziegler, USA). Starting $^{232}Th^{4+}$ solutions were prepared by direct dissolution of $Th(NO_3)_4 \cdot nH_2O$ salts purchased from Spex Industries (USA) and Strem Chemicals (USA). The age of the different ^{232}Th salts varied from ~0.5 to 20 years. Liquid scintillation and gamma analysis confirmed the presence of decay products. All aqueous solutions were prepared using deionized water purified by reverse osmosis. Buffers (VWR), non-radioactive chemicals (MilliporeSigma), PD-10 size exclusion columns (GE Healthcare), and Vivaspin® protein concentrators (Cytiva) were purchased and used as received. Wild-type LanM and LaMP1 were expressed and purified as previously described (*22*, *29*, *56*).

Radioanalysis. Liquid scintillation counting (LSC) was performed with a Perkin Elmer TriCarb 5110TR instrument equipped with an alpha/beta discriminator. Calibration was performed on a daily basis. Samples were diluted in UltimaGold^{TM} and results are background-corrected. Error bars displayed on the decay profile correspond to ±2σ unless otherwise indicated. Gamma analyses were

performed using high-purity Ge (HPGe) coaxial p-type semiconductor detectors, each rated at 21% and 37% standard efficiency relative to 3x3 NaI. Energy and efficiency calibrations were performed with NIST-traceable standards. Samples were counted as ~10 mL solutions in plastic vials (10 cm^2 cross sectional area) at distances of 4-5 cm from the face of the detector endcaps for up to 6 hours. Spectra were processed using GAMANAL (*57*).

Size exclusion separations. PD-10 columns prepacked with Sephadex G-25 media (8.3 mL, 5 kDa MWCO) and VivaSpin500 concentrators (membrane with 3 kDa MWCO) were pre-equilibrated with 5 bed volumes of buffer, as per the manufacturers' manuals. Sample volumes ranged from 0.4 to 3.0 mL. For thermodynamic measurements, samples were equilibrated at least 1 h before elution. For PD-10 columns, the sample was injected, followed by addition of buffer (~12 mL), and eluted by gravity. The elution lasts 5-10 min. The macromolecules elute at ~3 mL and the small molecules at ~6-9 mL. Individual fractions of 0.3 to 0.8 mL were collected and weighed for mass balance (0.1 mg accuracy). For spin filters, samples were centrifuged at 12,000×*g*, 20 min. Each fraction was radioanalyzed immediately after separation and monitored over time as needed. See below for radiopurity calculations.

Protein K_d determination by a radiometric- and dilution-based method. Solution thermodynamics stipulate that metal-ligand complexes dissociate at low concentrations:

$$Kd = \frac{[Metal]_{free} \times [Ligand]_{free}}{[Complex]}$$

In the presence of a large excess of ligand, $[Ligand]_{free} \approx [Ligand]_{total}$:

$$Kd = \frac{([Metal]_{total} - [Complex]) \times [Ligand]_{total}}{[Complex]}$$

$$[Complex] = \frac{[Ligand]_{total}}{Kd + [Ligand]_{total}} \times [Metal]_{total}$$

Size exclusion separations (pH 7.0, 10 mM HEPES + 90 mM NaCl, 22±0.5°C, PD-10) were performed with varying LanM and metal concentrations. The initial solutions of $^{228}Ac^{3+}/^{228}Ra^{2+}$ were aged 28 days to avoid any contamination with $^{224}Ra^{2+}$ and its daughters. At least 15

independent column separations were performed for both $^{90}Y^{3+}/^{90}Sr^{2+}$ and $^{228}Ac^{3+}/^{228}Ra^{2+}$ (12-15 fractions per column). Each fraction was measured over time by LSC to confirm the radionuclide identity. $^{90}Sr^{2+}$ and $^{228}Ra^{2+}$ were used as internal tracers. Each column separation allows determination of the fraction of bound and unbound Y^{3+} (Table S2) or Ac^{3+} (Figure 4e). As the metal and/or protein concentrations decrease, lower radiolabeling yields are observed for Y^{3+} and Ac^{3+}, albeit at different levels. Knowing the metal partition and the total concentrations, each column experiment allows evaluation of the formation of the metal-protein complex. Speciation calculations were performed with the computer program *HySS* (*58*) and taking into account the metal hydrolysis constants (*59*). Under the studied conditions the metal hydroxide species account for <1% for Ac^{3+} and <15% for Y^{3+}. The reported log $\beta(M_3LanM)$ are the average of at least 15 column experiments ($\pm 1\sigma$).

Protein K_d determination by CD. The conformational response of LanM in the presence of EGTA-buffered La^{3+} and EDDS-buffered Y^{3+} solutions was measured using circular dichroism as previously described (*22*).

Stability of La(III)-LaMP1 in serum. A solution of 10 mM $LaCl_3$ was added to 140 μM LaMP1 to a final metal:protein ratio of 2:1 and incubated at room temperature for 10 min. Buffer A (20 mM MOPS-KOH, 140 mM NaCl, pH 7.4, sterile filtered) and sterile-filtered human serum were individually incubated at 37° C. La(III)-LaMP1 or apo-LaMP1 was added to pre-warmed buffer A to 4 μM, mixed 1:1 with serum, and incubated at 37° C. At each time point, 100 μL of each reaction mixture was placed in a Greiner 96-well μCLEAR half-area plate and assayed on a BioTek Synergy H1 plate reader with 433 nm excitation and 460-550 nm emission (1 nm steps). FRET ratios were calculated by taking the ratio of an average of three wavelengths at the peak of each fluorophore emission (474-476 nm for ECFP and 528-530 nm for EYFP).

Radiopurity calculations. The purity of the ^{228}Ac and ^{90}Y fractions was evaluated based on the decay profile determined by LSC, using the total counts (0-2000 keV), to take into account all the

isotopes eventually present. Decay curves contained 25-65 time points, each corresponding to an LSC measurement and individual background. Decay curves were fitted with the following function.

$$A_{total} = A_{initial} \times e^{-\lambda \times t} + A_{Residual}$$

Since ^{90}Sr and ^{228}Ra have far longer half-lives than ^{90}Y and ^{228}Ac, their activity remains constant and can be determined from the residual activity after the decay of initial ^{90}Y and ^{228}Ac, respectively. Due to the secular equilibria ^{90}Sr/^{90}Y and ^{228}Ra/^{228}Ac, the residual activity corresponds to twice that of ^{90}Sr or ^{228}Ra, if present. For example:

$$A_{total} = {}^{228}Ac_{initial} + {}^{228}Ra + {}^{228}Ac_{regenerated}$$

$$A_{Residual} = {}^{228}Ac_{regenerated} + {}^{228}Ra = 2 \times {}^{228}Ra$$

The fitted values of $A_{initial}$ and $A_{residual}$ are directly linked to the purity of initial sample.

$$Radiopurity\ (t = 0) = \frac{A_{initial} - A_{Residual}/2}{A_{initial}}$$

SUPPLEMENTARY MATERIALS

Supplementary material for this article is available at [Insert link here].

REFERENCES AND NOTES

1. T. J. Wadas, E. H. Wong, G. R. Weisman, C. J. Anderson, Coordinating Radiometals of Copper, Gallium, Indium, Yttrium, and Zirconium for PET and SPECT Imaging of Disease. *Chem. Rev.* **110**, 2858–2902 (2010).

2. N. H. Álvarez, D. Bauer, J. Hernández-Gil, J. S. Lewis, Recent Advances in Radiometals for Combined Imaging and Therapy in Cancer. *ChemMedChem*. **n/a** (2021), doi:10.1002/cmdc.202100135.

3. E. Boros, A. B. Packard, Radioactive Transition Metals for Imaging and Therapy. *Chem. Rev.* **119**, 870–901 (2019).

4. E. Dolgin, Drugmakers go nuclear, continuing push into radiopharmaceuticals. *Nature Biotechnology*. **39**, 647–649 (2021).

5. N. A. Thiele, J. J. Woods, J. J. Wilson, Implementing f-Block Metal Ions in Medicine: Tuning the Size Selectivity of Expanded Macrocycles. *Inorg. Chem.* **58**, 10483–10500 (2019).

6. C. Kratochwil, F. Bruchertseifer, F. L. Giesel, M. Weis, F. A. Verburg, F. Mottaghy, K. Kopka, C. Apostolidis, U. Haberkorn, A. Morgenstern, 225Ac-PSMA-617 for PSMA-Targeted α-Radiation Therapy of Metastatic Castration-Resistant Prostate Cancer. *J Nucl Med*. **57**, 1941–1944 (2016).

7. F. Graf, J. Fahrer, S. Maus, A. Morgenstern, F. Bruchertseifer, S. Venkatachalam, C. Fottner, M. M. Weber, J. Huelsenbeck, M. Schreckenberger, B. Kaina, M. Miederer, DNA Double Strand Breaks as Predictor of Efficacy of the Alpha-Particle Emitter Ac-225 and the Electron Emitter Lu-177 for Somatostatin Receptor Targeted Radiotherapy. *PLOS ONE*. **9**, e88239 (2014).

8. M. R. McDevitt, D. L. J. Thorek, T. Hashimoto, T. Gondo, D. R. Veach, S. K. Sharma, T. M. Kalidindi, D. S. Abou, P. A. Watson, B. J. Beattie, O. V. Timmermand, S.-E. Strand, J. S. Lewis, P. T. Scardino, H. I. Scher, H. Lilja, S. M. Larson, D. Ulmert, Feed-forward alpha particle radiotherapy ablates androgen receptor-addicted prostate cancer. *Nat Commun*. **9**, 1–11 (2018).

9. M. Miederer, D. A. Scheinberg, M. R. McDevitt, Realizing the potential of the Actinium-225 radionuclide generator in targeted alpha particle therapy applications. *Advanced Drug Delivery Reviews*. **60**, 1371–1382 (2008).

10. C. Parker, S. Nilsson, D. Heinrich, S. I. Helle, J. M. O'Sullivan, S. D. Fosså, A. Chodacki, P. Wiechno, J. Logue, M. Seke, A. Widmark, D. C. Johannessen, P. Hoskin, D. Bottomley, N. D. James, A. Solberg, I. Syndikus, J. Kliment, S. Wedel, S. Boehmer, M. Dall'Oglio, L. Franzén, R. Coleman, N. J. Vogelzang, C. G. O'Bryan-Tear, K. Staudacher, J. Garcia-Vargas, M. Shan, Ø. S. Bruland, O. Sartor, Alpha Emitter Radium-223 and Survival in Metastatic Prostate Cancer. *New England Journal of Medicine*. **369**, 213–223 (2013).

11. K. Wickstroem, U. B. Hagemann, V. Cruciani, A. M. Wengner, A. Kristian, C. Ellingsen, G. Siemeister, R. M. Bjerke, J. Karlsson, O. B. Ryan, L. Linden, D. Mumberg, K. Ziegelbauer, A. S. Cuthbertson, Synergistic Effect of a Mesothelin-Targeted 227Th Conjugate in Combination with DNA Damage Response Inhibitors in Ovarian Cancer Xenograft Models. *Journal of Nuclear Medicine*. **60**, 1293–1300 (2019).

12. M. G. Ferrier, E. R. Batista, J. M. Berg, E. R. Birnbaum, J. N. Cross, J. W. Engle, H. S. L. Pierre, S. A. Kozimor, J. S. L. Pacheco, B. W. Stein, S. C. E. Stieber, J. J. Wilson, Spectroscopic and computational investigation of actinium coordination chemistry. *Nat Commun*. **7**, 1–8 (2016).

13. H. W. Kirby, L. R. Morss, in *The Chemistry of the Actinide and Transactinide Elements*, L. R. Morss, N. M. Edelstein, J. Fuger, Eds. (Springer Netherlands, Dordrecht, 2006; https://doi.org/10.1007/1-4020-3598-5_2), pp. 18–51.

14. F. Weigel, H. Hauske, The lattice constants of actinium(III) oxalate deca-hydrate. *Journal of the Less Common Metals*. **55**, 243–247 (1977).

15. G. J.-P. Deblonde, M. Zavarin, A. B. Kersting, The coordination properties and ionic radius of actinium: A 120-year-old enigma. *Coordination Chemistry Reviews*. **446**, 214130 (2021).

16. A. K. H. Robertson, B. L. McNeil, H. Yang, D. Gendron, R. Perron, V. Radchenko, S. Zeisler, P. Causey, P. Schaffer, 232Th-Spallation-Produced 225Ac with Reduced 227Ac Content. *Inorg. Chem.* **59**, 12156–12165 (2020).

17. D. S. Abou, J. Pickett, J. E. Mattson, D. L. J. Thorek, A Radium-223 microgenerator from cyclotron-produced trace Actinium-227. *Applied Radiation and Isotopes*. **119**, 36–42 (2017).

18. R. Perron, D. Gendron, P. W. Causey, Construction of a thorium/actinium generator at the Canadian Nuclear Laboratories. *Applied Radiation and Isotopes*. **164**, 109262 (2020).

19. C. Apostolidis, R. Molinet, J. McGinley, K. Abbas, J. Möllenbeck, A. Morgenstern, Cyclotron production of Ac-225 for targeted alpha therapy. *Applied Radiation and Isotopes*. **62**, 383–387 (2005).

20. W. Yan, Mining Medical Isotopes from Nuclear Waste. *ACS Cent. Sci.* **6**, 827–829 (2020).

21. R. A. Boll, D. Malkemus, S. Mirzadeh, Production of actinium-225 for alpha particle mediated radioimmunotherapy. *Applied Radiation and Isotopes*. **62**, 667–679 (2005).

22. J. A. Cotruvo Jr., E. R. Featherston, J. A. Mattocks, J. V. Ho, T. N. Laremore, Lanmodulin: A Highly Selective Lanthanide-Binding Protein from a Lanthanide-Utilizing Bacterium. *J. Am. Chem. Soc.* **140**, 15056–15061 (2018).

23. Y. Ye, H.-W. Lee, W. Yang, S. Shealy, J. J. Yang, Probing Site-Specific Calmodulin Calcium and Lanthanide Affinity by Grafting. *J. Am. Chem. Soc.* **127**, 3743–3750 (2005).

24. J. J. Yang, J. Yang, L. Wei, O. Zurkiya, W. Yang, S. Li, J. Zou, Y. Zhou, A. L. W. Maniccia, H. Mao, F. Zhao, R. Malchow, S. Zhao, J. Johnson, X. Hu, E. Krogstad, Z.-R. Liu, Rational Design of Protein-Based MRI Contrast Agents. *J. Am. Chem. Soc.* **130**, 9260–9267 (2008).

25. T. H. Flo, K. D. Smith, S. Sato, D. J. Rodriguez, M. A. Holmes, R. K. Strong, S. Akira, A. Aderem, Lipocalin 2 mediates an innate immune response to bacterial infection by sequestrating iron. *Nature*. **432**, 917–921 (2004).

26. P. A. Seeger, S. E. Rokop, P. D. Palmer, S. J. Henderson, D. E. Hobart, J. Trewhella, Neutron Resonance Scattering Shows Specific Binding of Plutonium to the Calcium-Binding Sites of the Protein Calmodulin and Yields Precise Distance Information. *J. Am. Chem. Soc.* **119**, 5118–5125 (1997).

27. M. P. Jensen, D. Gorman-Lewis, B. Aryal, T. Paunesku, S. Vogt, P. G. Rickert, S. Seifert, B. Lai, G. E. Woloschak, L. Soderholm, An iron-dependent and transferrin-mediated cellular uptake pathway for plutonium. *Nat Chem Biol*. **7**, 560–565 (2011).

28. B. E. Allred, P. B. Rupert, S. S. Gauny, D. D. An, C. Y. Ralston, M. Sturzbecher-Hoehne, R. K. Strong, R. J. Abergel, Siderocalin-mediated recognition, sensitization, and cellular uptake of actinides. *PNAS*. **112**, 10342–10347 (2015).

29. J. A. Mattocks, J. V. Ho, J. A. Cotruvo Jr., A Selective, Protein-Based Fluorescent Sensor with Picomolar Affinity for Rare Earth Elements. *J. Am. Chem. Soc.* **141**, 2857–2861 (2019).

30. G. J.-P. Deblonde, J. A. Mattocks, D. M. Park, D. W. Reed, J. A. Cotruvo Jr., Y. Jiao, Selective and Efficient Biomacromolecular Extraction of Rare-Earth Elements using Lanmodulin. *Inorg. Chem.* **59**, 11855–11867 (2020).

31. B. J. Tickner, G. J. Stasiuk, S. B. Duckett, G. Angelovski, The use of yttrium in medical imaging and therapy: historical background and future perspectives. *Chem. Soc. Rev.* **49**, 6169–6185 (2020).

32. C. L. Wright, J. Zhang, M. F. Tweedle, M. V. Knopp, N. C. Hall, Theranostic Imaging of Yttrium-90. *BioMed Research International*. **2015**, e481279 (2015).

33. *Therapeutic Radionuclide Generators: 90Sr/90Y and 188W/188Re Generators* (INTERNATIONAL ATOMIC ENERGY AGENCY, Vienna, 2009; https://www.iaea.org/publications/8045/therapeutic-radionuclide-generators-90sr/90y-and-188w/188re-generators), *Technical Reports Series*.

34. S. Shinoda, H. Tsukube, in *Encyclopedia of Metalloproteins*, R. H. Kretsinger, V. N. Uversky, E. A. Permyakov, Eds. (Springer, New York, NY, 2013; https://doi.org/10.1007/978-1-4614-1533-6_220), pp. 1087–1091.

35. G. J.-P. Deblonde, M. Sturzbecher-Hoehne, A. B. Mason, R. J. Abergel, Receptor recognition of transferrin bound to lanthanides and actinides: a discriminating step in cellular acquisition of f-block metals. *Metallomics*. **5**, 619–626 (2013).

36. A. G. Kazakov, B. L. Garashchenko, R. Yu. Yakovlev, S. E. Vinokurov, S. N. Kalmykov, B. F. Myasoedov, Generator of Actinium-228 and a Study of the Sorption of Actinium by Carbon Nanomaterials. *Radiochemistry*. **62**, 592–598 (2020).

37. K. E. Aldrich, M. N. Lam, C. Eiroa-Lledo, S. A. Kozimor, L. M. Lilley, V. Mocko, B. W. Stein, Preparation of an Actinium-228 Generator. *Inorg. Chem.* **59**, 3200–3206 (2020).

38. C. K. Luk, Study of the nature of the metal-binding sites and estimate of the distance between the metal-binding sites in transferrin using trivalent lanthanide ions as fluorescent probes. *Biochemistry*. **10**, 2838–2843 (1971).

39. H. Sun, H. Li, P. J. Sadler, Transferrin as a Metal Ion Mediator. *Chem. Rev.* **99**, 2817–2842 (1999).

40. A. R. Chipperfield, D. M. Taylor, Binding of Plutonium and Americium to Bone Glycoproteins. *Nature*. **219**, 609–610 (1968).

41. G. J.-P. Deblonde, M. Sturzbecher-Hoehne, P. B. Rupert, D. D. An, M.-C. Illy, C. Y. Ralston, J. Brabec, W. A. de Jong, R. K. Strong, R. J. Abergel, Chelation and stabilization of berkelium in oxidation state +IV. *Nature Chemistry*. **9**, 843–849 (2017).

42. M. P. Kelley, N. P. Bessen, J. Su, M. Urban, S. I. Sinkov, G. J. Lumetta, E. R. Batista, P. Yang, J. C. Shafer, Revisiting complexation thermodynamics of transplutonium elements up to einsteinium. *Chem. Commun.* **54**, 10578–10581 (2018).

43. S. Leguay, T. Vercouter, S. Topin, J. Aupiais, D. Guillaumont, M. Miguirditchian, P. Moisy, C. Le Naour, New Insights into Formation of Trivalent Actinides Complexes with DTPA. *Inorg. Chem.* **51**, 12638–12649 (2012).

44. T. P. Makarova, G. S. Sinitsyna, A. V. Stepanov, I. A. Shestakova, B. I. Shestakova, Complex formation of actinium. I. Determination of the stability constants of ethylenediaminetetraacetate complexes of actinium and its separation from lanthanum in solutions of EDTA by the method of electromigration. *Soviet Radiochemistry*. **14**, 555–557 (1972).

45. E. C. Cook, E. R. Featherston, S. A. Showalter, J. A. Cotruvo Jr., Structural Basis for Rare Earth Element Recognition by *Methylobacterium extorquens* Lanmodulin. *Biochemistry*. **58**, 120–125 (2019).

46. N. A. Thiele, J. J. Wilson, Actinium-225 for Targeted α Therapy: Coordination Chemistry and Current Chelation Approaches. *Cancer Biotherapy and Radiopharmaceuticals*. **33**, 336–348 (2018).

47. A. Hu, S. N. MacMillan, J. J. Wilson, Macrocyclic Ligands with an Unprecedented Size-Selectivity Pattern for the Lanthanide Ions. *J. Am. Chem. Soc.* **142**, 13500–13506 (2020).

48. L. M. De León-Rodríguez, Z. Kovacs, The Synthesis and Chelation Chemistry of DOTA−Peptide Conjugates. *Bioconjugate Chem.* **19**, 391–402 (2008).

49. M. Pérez-Malo, G. Szabó, E. Eppard, A. Vagner, E. Brücher, I. Tóth, A. Maiocchi, E. H. Suh, Z. Kovács, Z. Baranyai, F. Rösch, Improved Efficacy of Synthesizing *MIII-Labeled DOTA Complexes in Binary Mixtures of Water and Organic Solvents. A Combined Radio- and Physicochemical Study. *Inorg. Chem.* **57**, 6107–6117 (2018).

50. S. A. Greenberg, Zinc Transmetallation and Gadolinium Retention after MR Imaging: Case Report. *Radiology*. **257**, 670–673 (2010).

51. L. Telgmann, C. A. Wehe, J. Künnemeyer, A.-C. Bülter, M. Sperling, U. Karst, Speciation of Gd-based MRI contrast agents and potential products of transmetalation with iron ions or parenteral iron supplements. *Anal Bioanal Chem*. **404**, 2133–2141 (2012).

52. A. Turyanskaya, M. Rauwolf, V. Pichler, R. Simon, M. Burghammer, O. J. L. Fox, K. Sawhney, J. G. Hofstaetter, A. Roschger, P. Roschger, P. Wobrauschek, C. Streli, Detection and imaging of gadolinium accumulation in human bone tissue by micro- and submicro-XRF. *Sci Rep*. **10**, 1–9 (2020).

53. N. Bauer, D. R. Fröhlich, P. J. Panak, Interaction of Cm(III) and Am(III) with human serum transferrin studied by time-resolved laser fluorescence and EXAFS spectroscopy. *Dalton Trans.* **43**, 6689–6700 (2014).

54. B. W. Stein, A. Morgenstern, E. R. Batista, E. R. Birnbaum, S. E. Bone, S. K. Cary, M. G. Ferrier, K. D. John, J. L. Pacheco, S. A. Kozimor, V. Mocko, B. L. Scott, P. Yang, Advancing Chelation Chemistry for Actinium and Other +3 f-Elements, Am, Cm, and La. *J. Am. Chem. Soc.* **141**, 19404–19414 (2019).

55. E. A. Christenson, J. Schijf, Stability of YREE complexes with the trihydroxamate siderophore desferrioxamine B at seawater ionic strength. *Geochimica et Cosmochimica Acta*. **75**, 7047–7062 (2011).

56. E. R. Featherston, J. A. Mattocks, J. L. Tirsch, J. A. Cotruvo Jr., in *Methods in Enzymology*, J. A. Cotruvo Jr., Ed. (Academic Press, 2021; https://www.sciencedirect.com/science/article/pii/S0076687921000859), vol. 650 of *Rare-Earth Element Biochemistry: Methanol Dehydrogenases and Lanthanide Biology*, pp. 119–157.

57. R. Gunnink, W. D. Ruhter, J. B. Niday, "Operations guide for GRPANL (GRouP ANaLysis): A suite of computer programs for analyzing complex Ge and alpha-particle detector spectra: Volume 2" (UCRL-53861-Vol.2, Lawrence Livermore National Lab., CA (USA), 1988), (available at https://www.osti.gov/biblio/6775430).

58. L. Alderighi, P. Gans, A. Ienco, D. Peters, A. Sabatini, A. Vacca, Hyperquad simulation and speciation (HySS): a utility program for the investigation of equilibria involving soluble and partially soluble species. *Coordination Chemistry Reviews*. **184**, 311–318 (1999).

59. P. L. Brown, C. Ekberg, in *Hydrolysis of Metal Ions* (John Wiley & Sons, Ltd, 2016; https://onlinelibrary.wiley.com/doi/abs/10.1002/9783527656189.ch9), pp. 325–432.

60. R. D. Shannon, Revised Effective Ionic Radii and Systematic Studies of Interatomic Distances in Halides and Chaleogenides. *Acta crystallographica*. **A32**, 751–767 (1976).

61. G. J.-P. Deblonde, A. Ricano, R. J. Abergel, Ultra-selective ligand-driven separation of strategic actinides. *Nat Commun*. **10**, 2438 (2019).

62. S. G. Johnson, *NIST46 - NIST Critically Selected Stability Constants of Metal Complexes:* (2013; https://www.nist.gov/srd/nist46).

Acknowledgments: The authors thank Dr. Keenan J. Thomas (LLNL) for help with the gamma analyses and helpful discussions. The authors also thank Dr. Yongqin Jiao and Dr. Dan Park (LLNL) for comments on the manuscript and fruitful discussions.

Funding: This work was performed under the auspices of the U.S. Department of Energy (DOE) by Lawrence Livermore National Laboratory under Contract DE-AC52-07NA27344 (LLNL-JRNL-822758) and was supported by the LLNL-LDRD Program under Project No. 20-LW-017. J.A.M. and J.A.C. were supported by DOE grant DE-SC0021007.

Author contributions: GJPD and JAC conceived and designed the experiments. GJPD, JAM, ZD, PTW, and JAC performed the experiments. Funding acquisition: GJPD, JAC, and MZ. GJPD and JAC drafted the manuscript. All authors reviewed, edited, and approved the manuscript.

Competing interests: The authors declare the following competing financial interests: GJPD, JAM, ZD, and JAC are inventors on a patent application related to this work filed by Lawrence Livermore National Laboratory and the Pennsylvania State University (NO. 62/976,149, Filed on 02/13/2020). The authors declare no other competing interests.

Data and materials availability: All data needed to evaluate the conclusions in the paper are present in the paper and/or the Supplementary Materials. Materials for expression of lanmodulin and LaMP1 can be provided by J.A.C. pending scientific review and a completed material transfer agreement. Requests for these materials should be submitted to J.A.C.

FIGURES AND TABLES

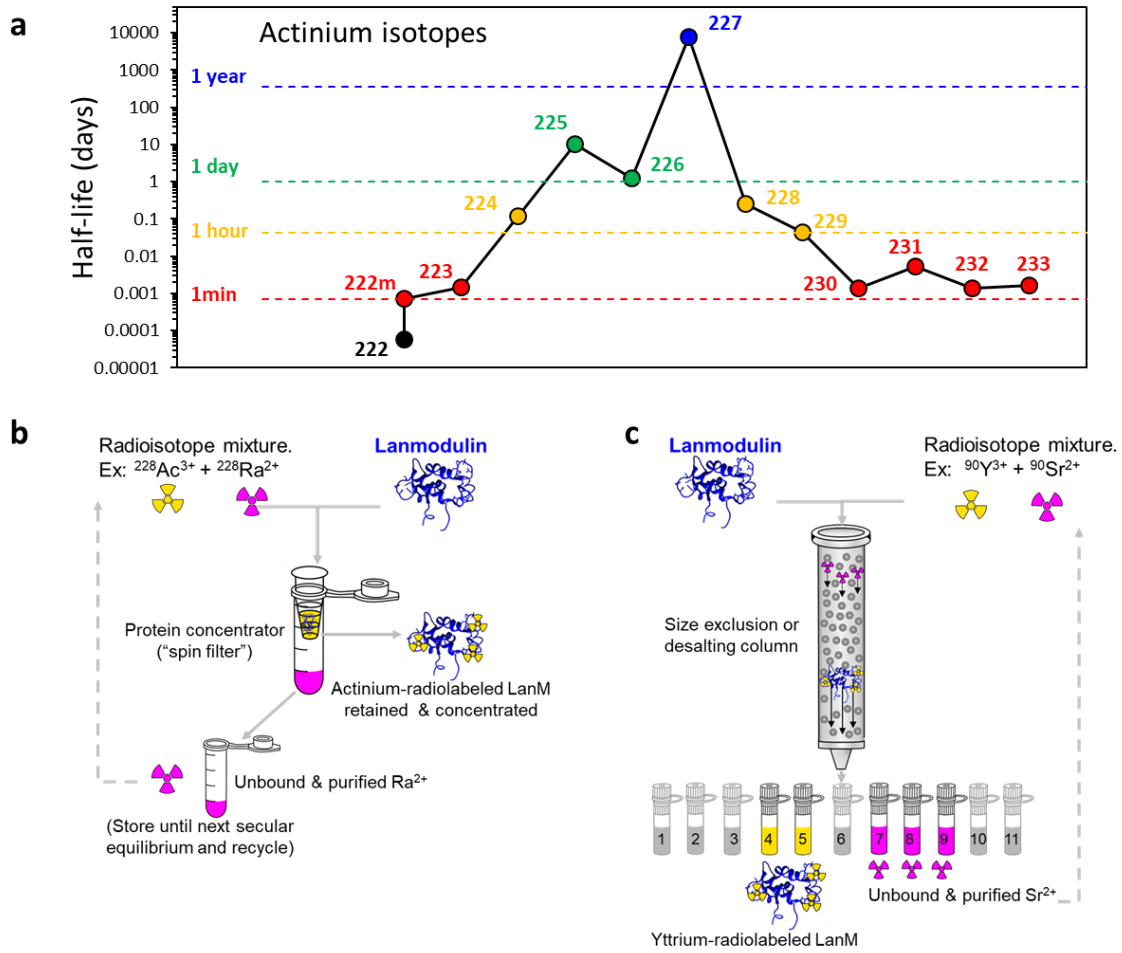

Figure 1. Actinium isotopes and protein-based radiometal recovery.
a, Half-lives of known actinium isotopes. ^{225}Ac is the principal actinium isotope studied for targeted-alpha therapies. ^{227}Ac is a research isotope and only produced at the microgram scale. Traces of ^{227}Ac are also present in aged ^{235}U or ^{231}Pa materials. ^{228}Ac occurs in the decay chain of natural thorium (^{232}Th) at very low concentrations, requiring a highly efficient extraction system. The other isotopes are short-lived and rarely studied. **b**, Principle of the lanmodulin (LanM)-based one-step radioisotope separation method via centrifugation using the so-called "spin filters" or "protein concentrators". In this configuration, the protein is retained with the target isotope (Y^{3+}, Ac^{3+}…) while the low molecular weight fraction is eluted. The filtrates contain the purified unbound metals (e.g., radium, strontium, thorium). **c**, LanM-based metal separation performed using a size exclusion column (also called "desalting column"). In this configuration, the radiolabeled lanmodulin elutes prior to the unbound metals. The separation can be performed by gravity elution, pumped elution, or centrifugation. In both **b** and **c** scenarios, no matrix change or acidity adjustment is needed to recover the elements in separate fractions. The radiometal can be desorbed from LanM by decreasing pH (<2) or adding a chelator in excess.

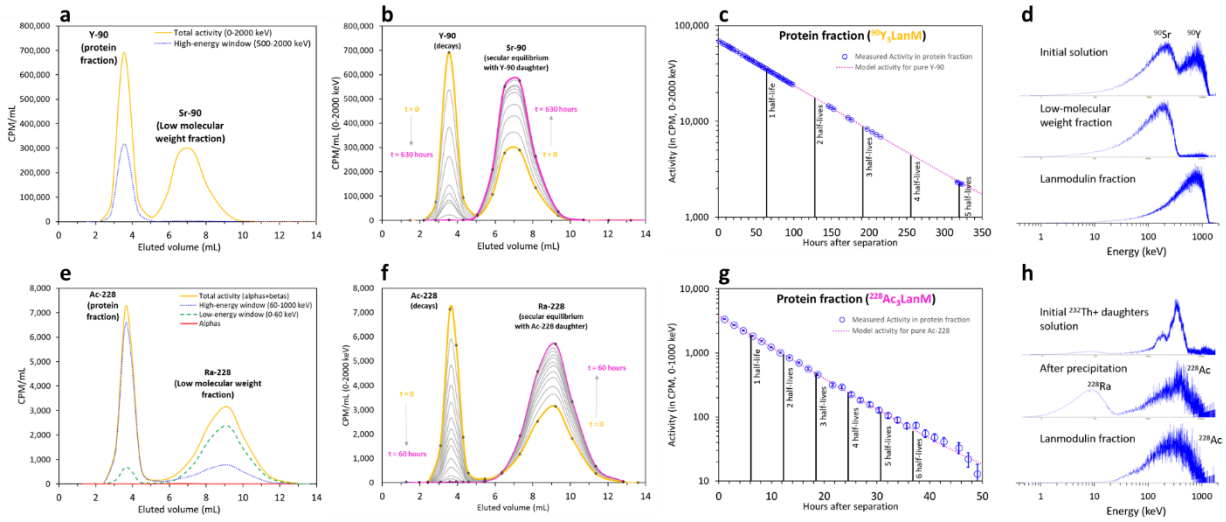

Figure 2. One-step extraction and purification of yttrium and actinium using LanM.
a, Typical elution profile of an ^{90}Sr/^{90}Y solution, initially at secular equilibrium, in the presence of LanM. [LanM] = 50 µM. Activity = 37 kBq/mL (1 µCi/mL). Buffer: 90 mM NaCl, 10 mM HEPES, pH = 7.0. **b**, **c**, Activity profile monitored at regular intervals, confirming the presence of high-purity ^{90}Y in the LanM fraction and quantitative separation ^{90}Sr/^{90}Y. **d**, Energy spectra, measured by liquid scintillation, for the starting ^{90}Sr/^{90}Y solution (top), the low-molecular weight fraction (middle), and LanM fraction (bottom). Spectra are normalized to the count maxima. **e**, Typical elution profile of a ^{228}Ra/^{228}Ac solution, initially at secular equilibrium, in the presence of LanM. [LanM] = 25 µM. Buffer: 90 mM NaCl, 10 mM HEPES, pH = 7.0. Note that pure ^{228}Ac inherently gives some counts in the low-energy window (green curve) due to the continuous nature of the beta emission. **f**, **g**, Activity profile monitored at regular intervals, confirming the presence of high-purity ^{228}Ac in the LanM fraction (Error bars or marker size = 2σ). **h**, Typical energy spectra of a solution containing the ^{232}Th decay chain (top), the solution after hydroxide precipitation (middle), and the purified ^{228}Ac fraction using the LanM-based method (bottom).

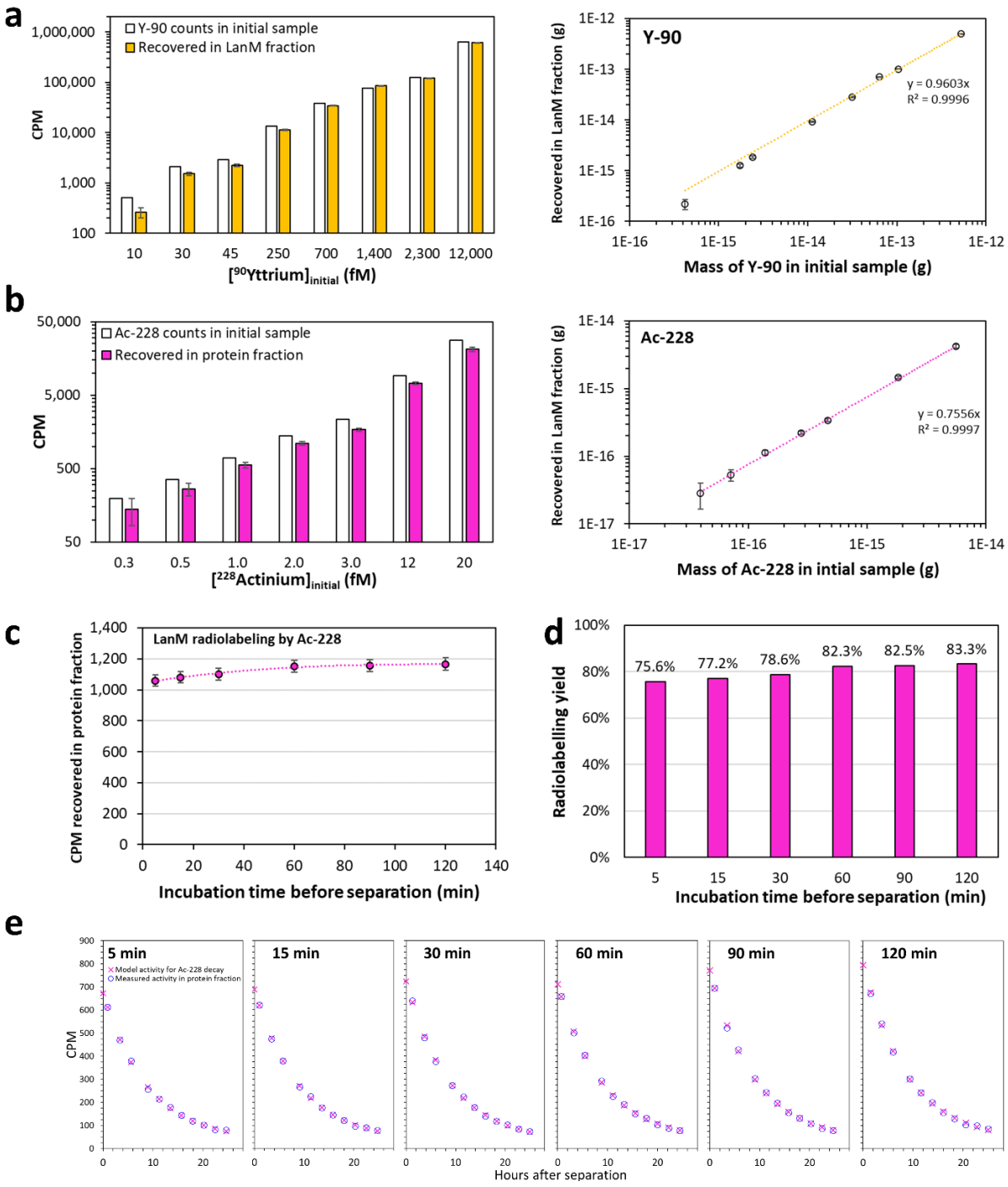

Figure 3. Recovery of Y and Ac radioisotopes at ultra-low levels.
a, Activity and mass of ^{90}Y recovered in the protein fraction, compared to the total initial amount, following a single-step elution of ^{90}Sr/^{90}Y samples at various concentrations. [LanM] = 1 µM. pH = 7.0. **b,** Similar experiments with ^{228}Ra/^{228}Ac samples. **c**, **d**, Activity recovered in the protein fraction and radiolabeling yield following a single-step elution of ^{228}Ra/^{228}Ac samples, as a function of the incubation period. [LanM] = 10 µM. Room temperature. Buffer: 10 mM HEPES, 90 mM NaCl, pH 7. **e**, Radioactive decay curve of the protein fractions obtained following different incubation periods (5 to 120 min) and elution through a size-exclusion column. The model radioactive decay for pure ^{228}Ac (crosses) is plotted for comparison with the experimental data (circles). The error bars correspond to ±3σ.

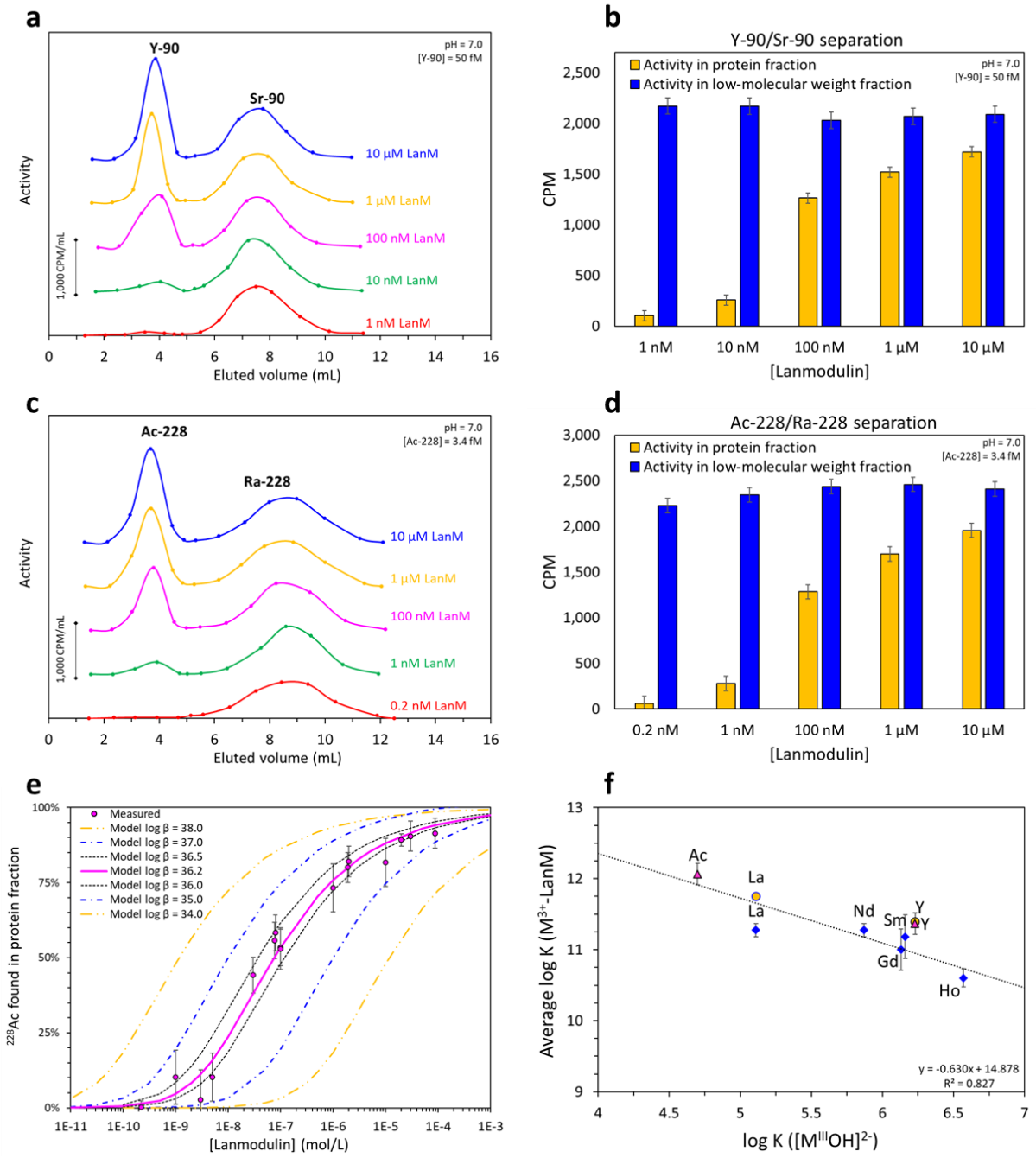

Figure 4. Stability of the actinium-lanmodulin complex.
a, Examples of elution profiles obtained with $^{90}Y/^{90}Sr$ at various concentrations of LanM. Buffer: 10 mM HEPES, 90 mM NaCl, pH 7.0, 22 °C. Size exclusion column: Sephadex PD-10 (5 kDa MWCO). **b**, Radioactivity detected in the low-molecular-weight fraction (^{90}Sr) and protein fraction (^{90}Y) as a function of LanM concentration. **c**, Examples of elution profiles obtained with $^{228}Ac/^{228}Ra$ at various concentrations of LanM. Conditions similar to the $^{90}Y/^{90}Sr$ experiments. **d**, Radioactivity detected in the low-molecular-weight fraction (^{228}Ra) and protein fraction (^{228}Ac) as a function of LanM concentration. **e**, Comparison of the experimental results and speciation models comprising $^{228}Ac_3$LanM with various stability constants, covering 4 orders of magnitude. The best fit of the experimental results is for log $\beta_{31}(^{228}Ac_3LanM) = 36.2$. **f**, Correlation between the Lewis acidity of the cations and the stability of their complexes with LanM. The average K_d per site is plotted against the first hydrolysis constant of the cation. The points for Ac^{3+} and Y^{3+} in magenta correspond to the radiochemical method; the points for La^{3+} and Y^{3+} in gold correspond to the CD method. Previous data (CD, pH 7.2) (*22*) are in blue. A similar correlation is given for transferrin in Figure S19.

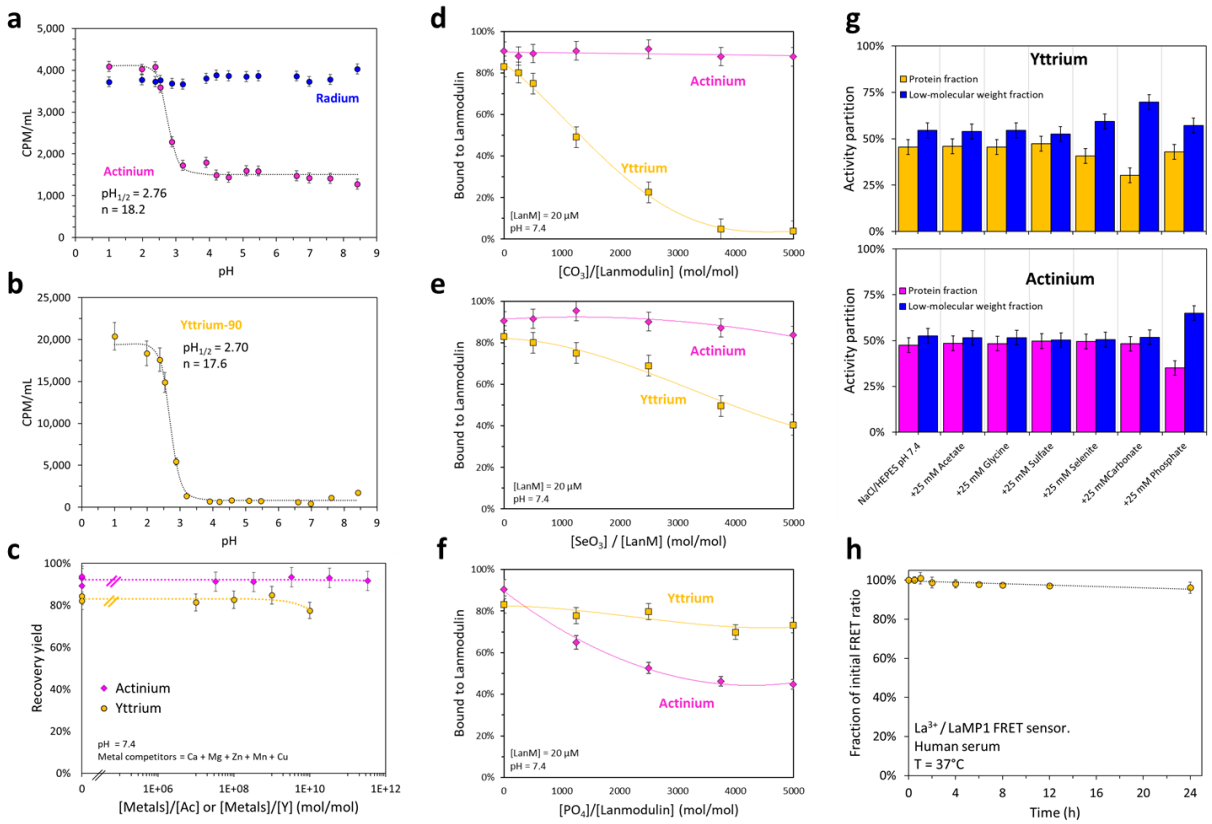

Figure 5. Solution chemistry of actinium in the presence of LanM.
a, Activity detected in the low-molecular-weight fraction as a function of pH, after filtration (20 min, 12,000×*g*, VivaSpin 3 kDa) of ^{228}Ra/^{228}Ac solutions, initially at secular equilibrium. 22 °C. I = 0.1M (NaCl). The dotted line corresponds to the fit using the Hill equation (*n* = Hill coefficient). **b**, Same experiments with ^{90}Y. **c**, ^{228}Ac or ^{90}Y recovered in the LanM fraction in the presence of Ca^{2+}, Mg^{2+}, Mn^{2+}, Zn^{2+}, and Cu^{2+}. The x-axis value is the concentration of each metal. PD-10 column, 20 µM LanM, 10 mM HEPES, 90 mM NaCl, pH 7.4. **d**, Percentage of ^{228}Ac and ^{90}Y bound to LanM in the presence of carbonate ions. pH 7.4, 10 mM HEPES, 90 mM NaCl, 0 to 100 mM $NaHCO_3$. **e**, **f**, Similar experiments in selenite and phosphate media. **g**, Activity partition in the presence of biorelevant anions. 20 µM LanM, pH 7.4, 90 mM NaCl, 10 mM HEPES, 25 mM biorelevant anions. ^{228}Ac and ^{90}Y experiments were done independently. Initial samples were at secular equilibrium. A perfect separation would yield 50% in each fraction. **h**, Stability of La^{3+}-bound complex of LaMP1 FRET sensor in 50% human serum. 2 µM LaMP1, 4 µM La, 37ºC. The raw FRET ratios are also given in Figure S21.